World Academy of Science, Engineering and Technology
International Journal of Geological and Environmental Engineering
Vol:3, No:5, 2009

Detailed Mapping of Pyroclastic Flow Deposits by SAR Data Processing for an Active Volcano in the Torrid Zone

Asep Saepuloh, and Katsuaki Koike

***Abstract*—**Field mapping activity for an active volcano mainly in the Torrid Zone is usually hampered by several problems such as steep terrain and bad atmosphere conditions. In this paper we present a simple solution for such problem by a combination Synthetic Aperture Radar (SAR) and geostatistical methods. By this combination, we could reduce the speckle effect from the SAR data and then estimate roughness distribution of the pyroclastic flow deposits. The main purpose of this study is to detect spatial distribution of new pyroclastic flow deposits termed as P-zone accurately using the β° data from two RADARSAT-1 SAR level-0 data. Single scene of Hyperion data and field observation were used for cross-validation of the SAR results. Mt. Merapi in central Java, Indonesia, was chosen as a study site and the eruptions in May-June 2006 were examined. The P-zones were found in the western and southern flanks. The area size and the longest flow distance were calculated as 2.3 km^2 and 6.8 km, respectively. The grain size variation of the P-zone was mapped in detail from fine to coarse deposits regarding the C-band wavelength of 5.6 cm.

***Keywords*—**Geostatistical Method, Mt. Merapi, Pyroclastic, RADARSAT-1.

I. Introduction

THE Torrid Zone weather conditions, such as heavy rain and thick clouds, prevent the application of optical remote sensing for monitoring and detection of new volcanic products such as pyroclastic flows, lava flows, and lahars. Thus, we used SAR (Synthetic Aperture Radar) microwave remote sensing, which has been used widely for monitoring active volcanoes (e.g., [1]-[4]). The superiority of SAR images is that they can provide periodic and synchronous Earth observations regardless of the time or weather.

Mt. Merapi, located in Central Java-Indonesia, was chosen as a study site (Fig. 1). This volcano has the most potential disaster due to a big city growth in the southwest flank. The eruptions of the Merapi volcano have frequently occurred with time intervals ranging from one to five years [5]. The eruptive activity is characterized by dome growth followed by extrusion of large amounts of pyroclastic flows.

Asep Saepuloh is a PhD student at Kumamoto University, 2-39-1 Kurokami, Kumamoto, Japan 860-8555 (phone: +81-080-5271-3897; e-mail: saepuloh@gmail.com). Katsuaki Koike is a Professor at Kumamoto University, 2-39-1 Kurokami, Kumamoto, Japan 860-8555 (e-mail:koike@gpo.kumamoto-u.ac.jp)

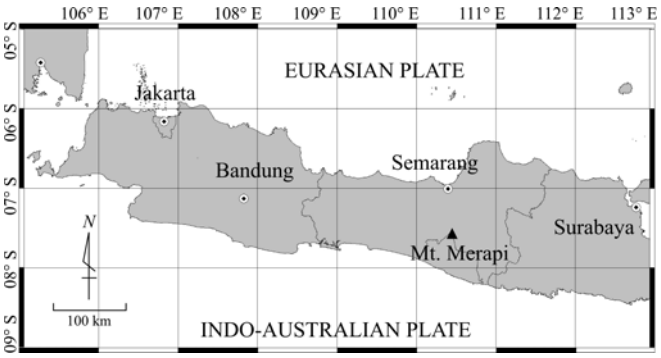

Fig. 1 Study location of Mt. Merapi in Central Java Indonesia

TABLE I
TWO RADARSAT-1 SAR DATA USED TO GENERATE β^{o} IMAGES

Orbit Date	Scene ID	Orbit	Off Nadir Angle
May 17, 2006	P0453701	Descending	32.9
July 04, 2006	P0458867	Descending	32.9

The latest eruptions were occurred during May-June 2006, which were similar to the previous historical eruption of Mt. Merapi, termed as Merapi Type.

In this study, we demonstrate the applicability of SAR backscatter data to delineate the detailed spatial distribution and estimate roughness of the P-zone supposed to be the pyroclastic flow deposits. Image processing of two scenes of RADARSAT-1 SAR level-0 data of descending mode with different acquisition dates and geostatistical methods were used. This level-0 product contains raw or unprocessed radar video baseband data in complex in-phase and quadrature signal (I and Q) format. The data acquisition dates are before and after the peak eruptions during May-June 2006. Details of the data are listed in Table I. A Hyperion data acquired on August 11, 2006 and a field survey including rock sample collection in December 2008 were used to check the detection results of the P-zone.

II. Image Processing of SAR Data for Detecting P-zone

Two RADARSAT-1 SAR level-0 data were processed using AV-APP 3.0, software from Atlantis Co. Inc., to generate Single Look Complex (SLC) data. After generation of SLC data, the radar brightness value (β°) for each image was calculated by the following equation:

$$\beta^0 = 10 * \log_{10}\left[\left(\frac{DNI_j}{A2_j}\right)^2 + \left(\frac{DNQ_j}{A2_j}\right)^2\right] \text{DB} \quad (1)$$

where DNI_j and DNQ_j are the digital values of the I and Q components at pixel, j, and $A2_j$ is the look-up table (LUT) value. The offset is not used in the SLC product generation [6].

Both the β° images were georeferenced and resampled using the nearest neighbor method. The β° images were subset to the field area, and forty ground control points were used for georeferencing with RMS error less than 0.2 pixel.

Radar backscatter is affected by three factors, local slope, roughness, and dielectric constant of material. In this study, the slope effect must be reduced; therefore we applied an arithmetical operation to reduce the effects in the β° images. Temporal changes of the β° images were extracted by calculating a ratio which allows emphasizing the large changes of the digital numbers; such changes represent generation of new volcanic products. Since the look angles of nadir of two RADARSAT-1 SAR data were same and only local deformation was occurred, slope component was assumed to be constant. Thus, by ratioing two β° images we obtained roughness and dielectric constant of material at surface. Fig. 2 shows two β° images and their ratio (R).

We should consider the image showing the geometric distortion by the slope effects such as foreshortening and layover that were occurred strongly near the summit (see Fig. 2A and B). Some ridges lied toward to the satellite has high bright value than the backward slope. This geometric distortion may cause an ambiguity when interpreting the data. However the ratioing can make this ambiguity negligible (see Fig. 2C). Therefore only the roughness and dielectric constant component influence the data. Based on this consideration we used R image for mapping the spatial distribution of the P-zone.

Isodata classification for the R image was adopted to reduce the speckle noises. The R image was classified into seven classes by variance parameter selected 0.2 for each class (see Fig. 3). This variance parameter was selected considering histogram of the R image. Based on the field survey during November 2008, we clarified that only two classes (class 1 and 7) were related to the P-zone and the other classes belonged to the other features such as vegetation, weathered lava flows, and lahars.

These two classes are produced by low and high bright value of R image. Theoretically, the P-zone should be located in the low R value (class 1) because the grain sizes of the P-zone are fine. However we also obtained the class 7 which has high bright value for the same rock type.

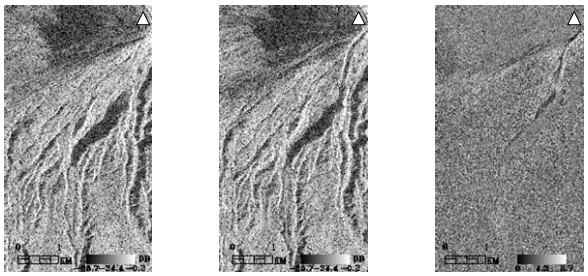

Fig. 2 (A) β^o images of RADARSAT-1 SAR data before, (B) after peak eruption, and (C) their ratio image, R. Radar look direction is to the left and white three angle symbol indicates the summit of Mt. Merapi

This phenomenon originated from the β° data with negative sign. After ratioing, they produced high bright value in the R image. In fact, these values belong to the P-zone. Fig. 4 shows a scatter graph of two β° data by blue rectangular symbols. Horizontal and vertical axes indicate the β° data after the peak eruption (July 4, 2006) and before it (May 17, 2006). Class 1 denoted by pink rectangular symbol is located lower than the class 7 (yellow triangle symbol). Linear regression was drawn for each class to show general trend in the scatter graph. The class 1 has the gradient gentler than class 7 because the β° values before the eruption are higher than after the eruption. Detailed explanation on the difference of bright values for the P-zone is discussed in the next chapter.

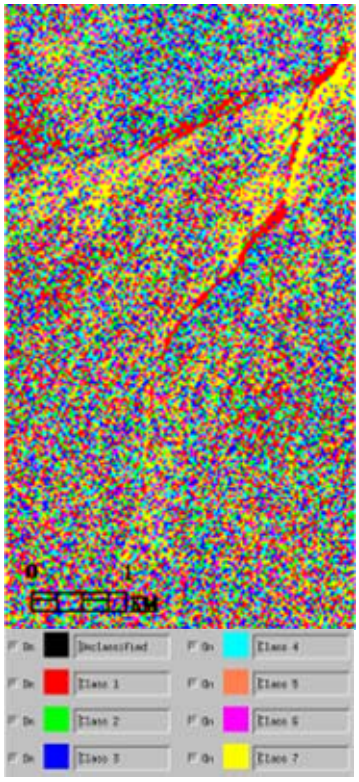

Fig. 3 Isodata classification of the R image. The P-zone is classified into two classes; class 1 (red) and 7 (yellow), respectively

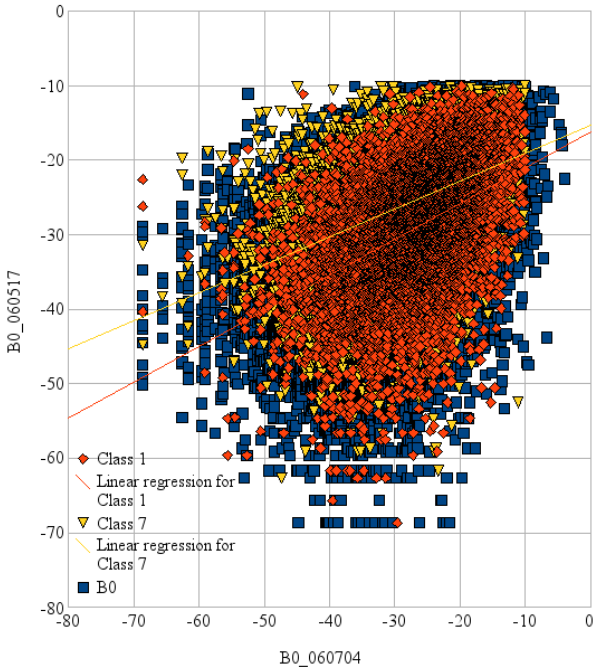

Fig. 4 Scatter graph of β° data pair where the P-zone located in two classes, class 1 and 7 of the *R* image

III. Detecting Spatial Distribution of P-zone

The purpose of this study is to produce a detailed spatial distribution map of the P-zones including their roughness degree. Geostatistical methods were applied to estimate the spatial distribution. Before this application, backscattering at a pixel size from the materials surrounding the P-zone must be considered because it produced speckles or noises in the *R* image. The speckles caused large nugget effect of the semivariogram. Therefore the P-zone could not be extracted correctly. To solve this problem, the *R* image was classified into seven classes as mentioned. Then, we used the mean value of each class, $\overline{R}_c$, defined as:

$$\overline{R}_c = I_R\left(\frac{1}{n}\sum_{i=1}^{n} c_i\right) \tag{2}$$

where *n* is sum of pixels belonging to each class, *c* is number of class, and I_R is Isodata classifier for the *R* image.

The $\overline{R}_c$ was assumed as a regionalized variable that is characterized by both random and spatial correlation aspects. Under the intrinsic hypothesis, both aspects can be quantified through the traditional semivariogram function:

$$\gamma(h) = \frac{1}{2}E\left[\overline{R}_c(x+h) - \overline{R}_c(x)\right]^2 \tag{3}$$

where $\gamma(h)$ represents half of the mathematical expectation of the quadratic increments of pixel pair values at a distance *h*.

Fig. 5 shows the histogram in logarithmic scale of *R* and the variogram of $\overline{R}_c$. Using the $\gamma(h)$, block kriging is applied to estimate the P-zone for window size 152×274(=1591) pixels.

Because the pixel values of the *R* image represent the average backscatter over the study area; block kriging is preferred algorithm for their interpolation [7]. Fig. 6 shows the resultant map of the $\overline{R}_c$ image, which clarifies that some high and low anomalies coincide with the locations of the P-zones. The color scale indicates relative roughness from May to June 2006. The coarse and fine grains are presented by low and high anomaly in the $\overline{R}_c$ image, respectively.

The high anomaly (more than 1.3) is originated from β° after the peak eruption on June 14, 2006. This β° has negative value smaller than the β° before the peak eruption: the area with has high anomaly probably has fine grain size by considering the wavelength 5.6 cm of C-band as compared to the low anomaly. On the contrary, the low anomaly (less than 0.9) is originated from coarse materials that were deposited after the peak eruption. The $\overline{R}_c$ value ranging from 0.9 to 1.3 correspond to the unchanged materials (constant in ratio). The area which has this value range was not affected significantly by the eruption.

The high and low anomalies mainly followed the two rivers (Krasak and Gendol) and were elongated from the summit toward southwest direction. Especially in the Gendol River, the P-zone is bent from southwest to the south. Energy of the eruption and local topography are suggested to be the main factors controlling the flows.

Considering the wavelength of C band, the vegetation also has relative to the $\overline{R}_c$ map. The large change of the vegetation caused the low anomaly in the $\overline{R}_c$ map, which is located in the lower right of Fig. 6. Two cross-section lines (A-B and C-D) were used to explain the variation of grain size in the following chapter.

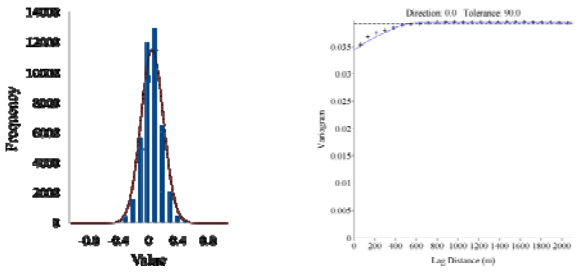

(A) (B)

Fig. 5 (A) Histogram of the *R* image with log normal distribution curve fitted to the histogram. (B) Omnidirectional experimental semivariogram of distribution of the $\overline{R}_c$ with the mean of each classes (B)

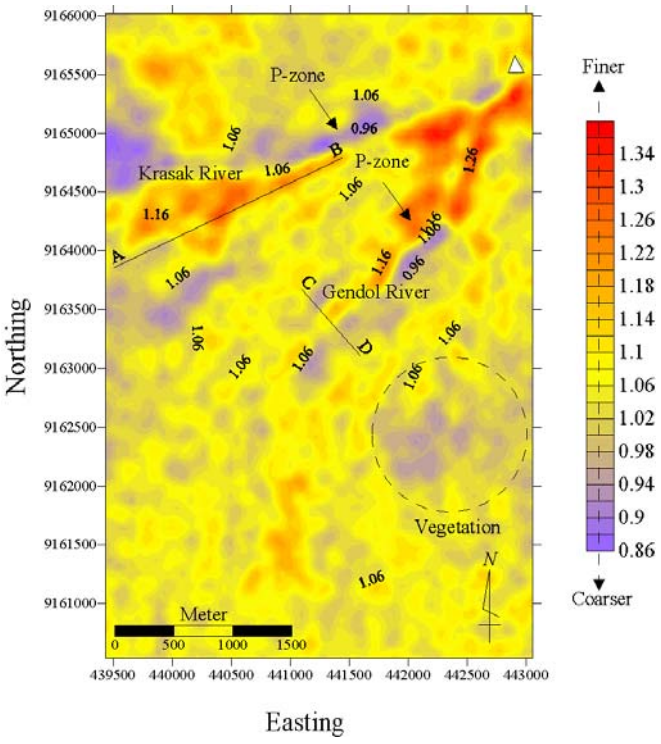

Fig. 6 Kriging estimation of the $\overline{R}_c$ image. Arrows indicate the P-zone which is located in the high and low anomaly, respectively

IV. Discussion

An important point of this paper is the superiority of SAR backscatter data for identifying materials based on the roughness. We found that the P-zone pertaining of the pyrolastic flow deposits had different bright values in the *R* image. This difference means difference of roughness degree rather than dielectric constant of material. The roughness is suggested to have high contribution than the dielectric constant because all materials detected are the same. To check this assumption, Spectral Angle Mapper (SAM) supervised classification was applied to the Hyperion data. We used end member spectra of three different rock types of the P-zone sampled by the field survey. The reflectance spectra of the samples were measured using SOLIDSPEC Spectrometer as shown in Fig. 7.

There are three rock types which were mapped successfully: new pyroclastic flows (NPF), old pyroclastic flows (OPF), and old lava dome (OLD). The NPF are the rocks formed by the explosion of the solidified magma with high gas content. The OPF is fragmented rocks that were deposited before the eruption and may be re-deposited after the eruption. The OLD is the fragmented rocks originated from the explosion of the lava dome that was formed by the previous eruptions. This rock type has been be re-deposited by several times eruption.

The P-zone detected by the SAR data consists of the three rock types. They are mixed near the summit and flowed toward the lower topography. Fragmental rocks from the OLD cover the P-zone widely and coincide with the high *R* values suggesting fine grain size (See Fig. 6). High energy of the eruption causes dome destruction and breaks the materials strongly into fine grain size accompanying materials flows from the summit.

Since the P-zone contains various rock types, the roughness degree may have a low relationship with the rock types. Therefore the $\overline{R}_c$ map contains information on spatial distribution of the roughness degree of the P-zone rather than the different rock types. The causes of variation in grain size are discussed from a viewpoint of internal and external factor controlling the flows.

The internal factor such as the energy of eruption is related to the pressure from the magma beneath the summit, which can cause the materials from the summit exploded variously in the grain size [8]. Low energy of eruption can produce coarser grain size than high energy of eruption. In the case of Mt. Merapi, the last eruption begun in May 2006 and the peak eruption was occurred on June 14, 2006 accompanying collapse of the dome on the summit. The energy of eruption was varied in this period. Based on information from Volcanological Survey of Indonesia (VSI), at the beginning stage of eruption, the pyroclastic flows devastated the area around the Krasak River (Fig. 6) on May 2006. This eruption is considered weaker than the peak eruption on Jun 14, 2006. Therefore coarse grains were deposited chiefly in this river. Moreover, based on the digital elevation model (DEM), the slope of the Krasak River is steeper (about 60˚) than the Gendol River (about 40˚).

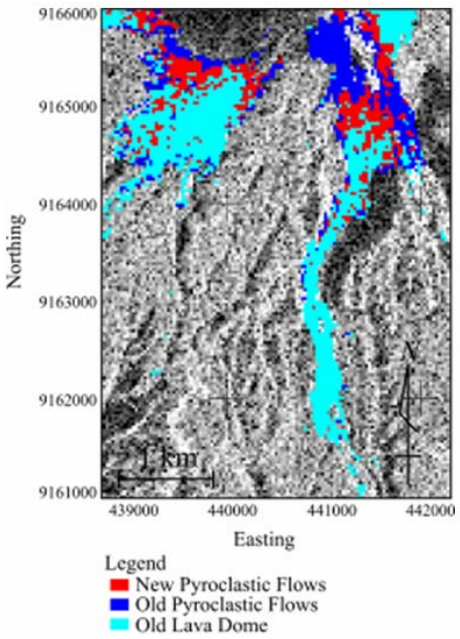

Fig. 7 Spectral Angle Mapper (SAM) classification result showing distribution of three different rock types overlaid on RADARSAT-1 β° data after geo-referencing

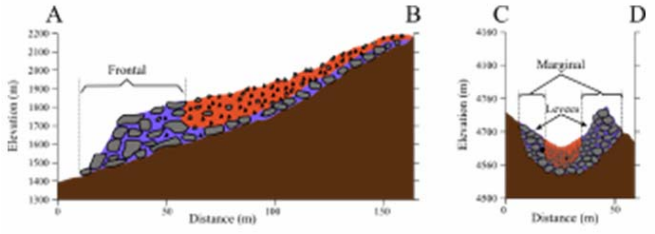

Fig. 8 Simplified vertical cross-section of the P-zone along A-B and C-D lines in Fig. 6 showing variation of grain size with distance and elevation

Low energy of the eruption in the beginning stage with high slope condition controlled the flows and caused the coarse grains accumulated in the lower part. In the Krasak River, the fine grains were also accumulated due to the depositional process rather than the eruption energy.

On the other hand, the fine materials can be found chiefly in the Gendol River which is presented by the high anomaly in the $\overline{R}_c$ image (Fig. 6). The pyroclastic flows devastated the Gendol River during the peak eruption on June 14, 2006. Fine grains were accumulated chiefly and flowed further due to the maximum energy of eruption.

The external factor such as depositional process may also affect the accumulation different of grain size. Generally, the fine grains of the P-zone is deposited and isolated in the centerline of coarse grains. This result is agreeable to depositional process of pyroclastic density currents [9], which reported that internally the pyroclastic flow deposits comprise three parts, a coarse-grained layer in bottom part that laterally connects to levees, an ashy matrix-supported layer in middle part, and an overlying coarse plaster layer in upper part. In our result, ashy matrix-supported layer in middle part and an overlying coarse plaster layer in upper layer are mixed. High local slope condition may cause this mixture. Thus SAR backscatter could not clarify the difference of significant values. However boundary between the coarse-grained and the ashy matrix-supported layer can be seen clearly.

The coarse grains as basal were accumulated in the bottom part of the fine grains in a vertical section. The coarse grains are concentrated in the frontal and marginal regions connected to levees. Fig. 8 shows simplified vertical cross-sections to explain variation of grain size with deep and distance. In A-B section, the coarse grains are accumulated in the bottom part and connected to the frontal part. The coarse grains are also connected to marginal part by creating levees along the path flows (C-D section). In total, the area size and the longest flow distance of the P-zone are calculated as 2.3 km^2 and 6.8 km, respectively. The longest flow distance is located in the Gendol River.

V. Conclusion

The capability of SAR backscatter data to identify the new pyroclastic flow deposits was proved regardless the atmospheric conditions. The pyroclastic flow deposits showed low bright value in the β° image due to low backscatter return to the satellite. However, after ratioing we obtained the low and high value of $\overline{R}_c$ image. These values correspond to the roughness degree of the pyroclastic flow deposits.

Detecting pyroclastic flow deposits using SAR β° image was improved by using geostatistical methods which allows generation detailed spatial distribution map including roughness degree of materials. Based on the result of SAM classification for Hyperion data and filed survey, the pyroclastic flows deposits consist of three different origins of rocks. Their distributions do not have direct relation to the roughness degree. Therefore SAR backscatter data is more effective to detect roughness degree than rock types.

Internal factor such as eruption energy, external factor such as depositional process, and local topographical condition had the influences on variation of the roughness distribution. Low energy of the eruption with high slope produced the fragmented materials deposited coarsely. On the contrary, high energy of the eruption with low slope caused the fine grain size deposited and distributed widely than the coarse materials. The coarse grains were flowed as basal and accumulated under the fine grains. The P-zone depositional process was interpreted as the pyroclastic density current in which the grain sizes are distributed variously with distance from the summit. The area size and the longest flow distance were calculated as 2.3 km^2 and 6.8 km, respectively, which mainly filled river banks.

References

[1] S. A. Carn, "Application of Synthetic Aperture Radar (SAR) imagery to volcano mapping in the humid tropics: A case study in East Java, Indonesia", Bulletin of Volcanology, vol. 61, 1999, pp. 92-105.
[2] D. Massonnet, P. Briole, and A. Arnaud, "Deflation of Mt. Etna monitored by spaceborne radar interferometry", Nature, vol. 375, 1995, pp567-570.
[3] F. Sigmundsson, P. Durnand, and D. Massonnet, "Opening of an eruptive fissure and seaward displacement at Piton de la Fournaise volcano measured by RADARSAT satellite radar interferometry", GRL, vol. 26, 1999, pp. 533-536.
[4] H.A. Zebker, P. Rosen, S. Hensley, and P. Mouginis-Mark, "Analysis of active lava flows on Kilauea volcano, Hawaii, using SIR-C radar correlation measurement", Geology, vol. 24, 1996, 495-498.
[5] B. Voight, E. K. Constantine, S. Siswowidjoyo, R. and Torley, "Historical eruptions of Merapi volcano, Central Java, Indonesia, 1768–1998", J. Vol. and Geoth. Res., vol. 100, 2000, pp. 69–138.
[6] N. Shepherd, "Extraction of beta nought and sigma nought from RADARSAT CDPF products", Report AS97-5001 Rev. 2, Canadian Space Agency, Ottawa, Ont., Canada, 1998.
[7] N. F. Glenn and J. R. Carr, "Establishing a relationship between soil moisture and RADARSAT-1 SAR data obtained over the Great Basin, Nevada, U.S.A.", Canadian Journal of Remote Sensing, Vol. 30, No. 2, 2004, pp. 176–181.
[8] R. F. Fudali and W. G. Melson, "Ejecta velocities, magma chamber pressure and kinetic energy associated with the 1968 eruption of Arenal volcano", Bulletin of Volcanology, vol. 35, 1971, pp. 383-401.
[9] G. Lube, S. J. Cronin, T. Platz, A. Freundt, J. N. Procter, C. Henderson, and M. F. Sheridan, "Flow and deposition of pyroclastic granular flows: a type example from the 1975 Ngauruhoe eruption, New Zealand", Journal of Volcanology and Geothermal Research, vol. 161, 2006, pp. 165-186.